



Chemically Inert Hydrocarbon-Based Slurries for Rapid Laser Sintering of Thin Proton-Conducting Ceramics

Akihiro Ishii^{a,1}, Hua Huang^a, Yuqing Meng^a, Shenglong Mu^a, Jun Gao^a, Jincheng Lei^b, Fei Peng^a, Hai Xiao^b, Jianhua Tong^{a,*}, Kyle S. Brinkman^{a,*}

^a Department of Materials Science and Engineering, Clemson University, SC 29634, USA

^b Department of Electrical and Computer Engineering, Clemson University, SC 29634, USA

ARTICLE INFO

Keywords:

Ceramic
Wet processing
Laser sintering
Proton conductor
Fuel cell

ABSTRACT

The process of rapid laser sintering of thin BaZrO₃-BaCeO₃-based proton-conducting electrolytes is being developed for easy fabrication of ceramic fuel cells and electrolyzers. However, cracks on the electrolytes caused by volume change due to chemical reactions between the basic ceramic constituents and the polar solvents during wet processing has been problematic. In order to address this issue, the use of chemically inert saturated-hydrocarbon-based slurries comprised of hexadecane, polybutene, and a long-chain saturated fatty acid were investigated in this work. By optimizing slurry composition and laser sintering conditions, a 20 mm long, 4 mm wide, 13.5- μ m-thick and 97%-dense BaCe_{0.7}Zr_{0.1}Y_{0.07}Sm_{0.13}O_{3-d} membrane showing proton conductivity on the order of 10⁻⁴ S \cdot cm⁻¹ at 600 °C was successfully prepared in just three seconds by laser sintering. The use of saturated-hydrocarbon-based slurries will facilitate wet processing and rapid laser sintering of proton-conducting ceramic electrolytes.

1. Introduction

Ceramic fuel cells and electrolyzer cells are key devices for a highly-efficient hydrogen economy with minimal environmental impact. Proton-conducting ceramics have attracted increased attention as solid electrolytes of these devices. The development of chemically stable proton-conducting ceramics showing higher proton conductivity and the development of processing technologies enabling easier fabrication of thin dense electrolyte membranes have been active areas of contemporary research. The material development has resulted in a number of promising systems such as BaZrO₃-BaCeO₃-based system: BaCe_{1-x-y}Zr_xY_yO_{3- δ} (BCZY) [1], BaCe_{0.7}Zr_{0.1}Y_{0.1}Yb_{0.1}O_{3- δ} (BCZYYb) [2], BaCe_{0.7}Zr_{0.1}Y_{0.07}Sm_{0.13}O_{3- δ} (BCZYSm) [3], and 60 mol% Sc-doped BaZrO₃ [4]. Even though the preparation of dense membranes of refractory BaZrO₃-BaCeO₃ based materials have become easier to some extent by discovery of solid state reactive sintering methods [5,6], the new processing technologies still need significant effort.

Among several next-generation processing technologies aimed at facile sintering of refractory ceramics (e.g. spark plasma sintering, microwave sintering, cold sintering), the authors have focused on laser

sintering technique because of its compatibility with membrane preparation and the ability for layer-by-layer fabrication of the single cells and cell stacks. [7–13] This technique uses an infrared laser to heat green ceramics sheets prepared *via* a wet process. Laser sintering has the advantage of increased speed: even refractory ceramics can be sintered in minutes or seconds. The authors have previously reported on laser sintering of ceramics membranes including BaZrO₃-BaCeO₃ solid-solution-based materials, and demonstrated that highly densified and conductive membranes as thin as ten-plus micrometers can be effectively prepared. [11,12]

One of the important keys to successful laser sintering is suppression of cracking. As the authors previously reported, ceramic membranes are frequently cracked by the laser sintering process. [12] The major reason is volume reduction during laser sintering as bulky hydroxides and/or carbonates (e.g. Ba(OH)₂, BaCO₃) turn to the oxides (e.g. BaZrO₃). These polyanion chemicals are formed from the original oxide precursors in accordance with thermodynamics. Fig. 1(a) shows changes of standard Gibbs energy, ΔG° , for decomposition of simple binary oxides to hydroxides in water. It shows that Ba²⁺, which is the most commonly used cation in the proton-conducting ceramics, strongly prefers to bond with

* Corresponding authors.

E-mail addresses: jianhut@clemson.edu (J. Tong), ksbrink@clemson.edu (K.S. Brinkman).

¹ Current affiliation: Department of Materials Science and Engineering, Tohoku University, Sendai 980–8579, Japan

OH^- rather than O^{2-} especially at slurry processing temperatures ($\approx 25^\circ\text{C}$). In reality, the $\text{Ba}(\text{OH})_2$ formed by its aqueous has to be greatly hydrated by taking it into account that $\text{Ba}(\text{OH})_2 \cdot 8\text{H}_2\text{O}$ is its most stable state in ambient air. Some portion of the resulting hydrated hydroxides of basic cations subsequently react to form carbonates readily by air exposure, which has been reported in many papers. [14–17] By the laser heating, dehydration and decarbonation reactions accompanied with harsh volume reduction are taken place, and thus, the membranes are cracked. Even using BaCO_3 as the precursor, the cracking has been less but still frequently observed. This suggests that the cracking is induced namely by the dehydration process since $\text{Ba}(\text{OH})_2 \cdot x\text{H}_2\text{O}$ is bulkier than BaCO_3 , and BaCO_3 that dissolved in water solidified partially as $\text{Ba}(\text{OH})_2 \cdot x\text{H}_2\text{O}$. It should be noted that the similar reactions on Ba-containing oxides by water are expected also in the cold sintering process and may severely impact on material properties, such as ferroelectricity of BaTiO_3 .

The thermodynamic analysis also revealed that compositional control on the proton-conducting ceramics for increasing their conductivity also increases the instability of the Ba-O bonding. Fig. 1(b) shows ΔG° for decomposition of BaZrO_3 and BaCeO_3 to $\text{Ba}(\text{OH})_2$, and ZrO_2 or CeO_2 in water. BaZrO_3 shows positive ΔG° even at room temperature, meanwhile, BaCeO_3 shows negative ΔG° . Since recent proton-conducting ceramics are modified to have a higher Ce:Zr ratio in order to achieve higher proton conductivity (cf. Ce:Zr in BCZYb and BCZYSm are 7:1 by molar) because of the reported lower proton conductivity in BaZrO_3 than in BaCeO_3 , it is reasonable that they readily decompose in water at around room temperature. Fig. 1(c) shows standard enthalpy changes at room temperature, $\Delta H^\circ_{298.15\text{K}}$, for decomposition of undoped and 20 mol%Y-doped BaZrO_3 to $\text{Ba}(\text{OH})_2$, ZrO_2 , and Y_2O_3 in water. Even for BaZrO_3 which exhibits well known chemical stability, $\Delta H^\circ_{298.15\text{K}}$ turns negative from positive at 20 mol%Y doping. This points out that acceptor doping for achieving higher proton concentration ($[\text{Y}'_{\text{Zr}}] = [\text{OH}_i]$) reduces the stability against water. Thus, there is a trade-off relationship between proton conductivity and chemical stability; therefore, chemically inert solvent that can protect the proton-conducting ceramics from water has to be explored for wet processing followed by laser sintering.

The reactions of ceramics with water have been a problem also in the field of alkali-ion batteries, and alternative compatible organic solvents have been explored. Alcohols [22,23], aromatic hydrocarbons [24–27], *n*-methyl-pyrrolidone (NMP) [28,29], and acetonitrile [30,31] are typical alternatives. However, alcohols become alkoxides while giving -OH to the basic ceramics, as suggested by Kun et al. [32] The aromatic hydrocarbons, such as xylene and toluene, are aprotic, however, controlling and maintaining a solid-liquid ratio of aromatic-hydrocarbon-based slurries is difficult because of their high vapor pressure. NMP and acetonitrile are aprotic solvents having

relatively low vapor pressure, however, they are highly hydrophilic and absorb water during handling in air. Tan et al. have reported that such polar organic solvents absorb air moisture immediately after the air exposure. [33] Kun et al. have reported that acetonitrile leads negligible reactions with a basic ceramic of Al-doped $\text{Li}_7\text{La}_3\text{Zr}_2\text{O}_{12}$; however, it was handled in a glovebox and was dehydrated carefully by molecular sieves presumably due to the hygroscopicity of acetonitrile. [32]

Taking prior work into account, slowly-evaporating, aprotic, and non-polar saturated higher *n*-hydrocarbons most likely be the best as solvents of slurries that minimize the propensity for cracking. The use of these types of solvent systems will also be beneficial from viewpoint of safety due to their relatively low toxicity in the human body and relatively high flash points ($>100^\circ\text{C}$). In spite of these benefits, hydrocarbon-based slurries have not been utilized to the best of the authors' knowledge. This is presumably because there are no reports about binders and surfactants that can be used with the saturated hydrocarbon systems. Popular binders and surfactants to date for the ceramic slurries are polar organics (e.g. PVB [22,24,25,27,34], PVP [35,36], PEO [30,31,37], cellulose derivatives [11,23] for binders; ethylene glycol [24,38], ammonium polyacrylates [11,39], octylphenol ethoxylates [22,40,41] for surfactants); therefore, they cannot be dissolved into the saturated hydrocarbons having exactly zero polarity.

In this paper, the compatibility of saturated higher *n*-hydrocarbon with the proton-conducting ceramics (BCZYSm: $\text{BaCe}_{0.7}\text{Zr}_{0.1}\text{Y}_{0.07}\text{Sm}_{0.13}\text{O}_{3-\delta}$) was studied, and the saturated-hydrocarbon-based BCZYSm slurry were developed by exploring binders and surfactants that can be dissolved into saturated higher hydrocarbons. Using the optimized slurry, laser sintering of proton-conducting BCZYSm membranes was demonstrated. The phase formation, microstructure and ion conductivity of the resulting materials are reported.

2. Experimental

Green and calcined BCZYSm slurries were prepared using a planetary ball mill at 400 rpm for 12 h using agate jars and balls for the compatibility test and for the laser sintering. The green BCZYSm powder is a stoichiometric mixture of BaCO_3 (Alfa Aesar, 99.8%), CeO_2 (Alfa Aesar, 99.9%), ZrO_2 (Alfa Aesar, 99.7%), Y_2O_3 (Alfa Aesar, 99.99%), Sm_2O_3 (Alfa Aesar, 99.9%). The calcined BCZYSm was prepared by calcining the green BCZYSm powder at 1400°C for 14 h.

For the compatibility tests, deionized water, isopropanol (Alfa Aesar, 99.5%), hexadecane (Acros Organics, 99%) based calcined BCZYSm slurries were prepared. The slurries were comprised of the calcined BCZYSm powder 10 g and the solvents 100 mL. The bottle of isopropanol was opened just before the test in order to minimize the contamination of water from air. The content of barium leaching from the calcined

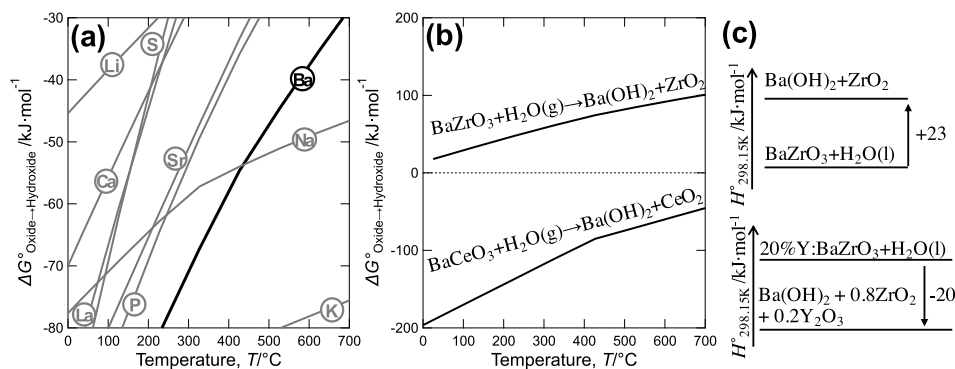


Fig. 1. Thermodynamic analysis about chemical reactivity of proton-conducting electrolytes calculated using references [18–21]: (a) change of standard Gibbs energy, ΔG° , for turning simple binary oxides to hydroxides in water, (b) ΔG° for decomposition reaction of BaZrO_3 and BaCeO_3 forming $\text{Ba}(\text{OH})_2$, and (c) change of standard enthalpy, ΔH° , for decomposition of undoped and 20 mol%Y-doped BaZrO_3 .

BCZYSm to the solvents was analyzed by an inductively coupled plasma mass spectrometry (ICP-MS). The slurries were centrifuged at 9500 rpm for 20 min and filtrated using polyethersulfone filters having 200 nm size pores beforehand.

The slurry for the laser reactive sintering was prepared by ball milling following materials: 1 wt%NiO-added green BCZYSm powder, hexadecane (solvent), polybutene (binder; Indopol® H-18,000, average $6000 \text{ g}\cdot\text{mol}^{-1}$, INEOS oligomers), stearic acid (surfactant; Alfa Aesar, 98%). Their detailed weight ratio is described in Results and Discussion section. NiO was added as the sintering aid. [6] The polybutene was mixed as hexadecane–polybutene one-to-one (by volume) solution for handling easily. This solution was prepared by mixing them at $50 \text{ }^\circ\text{C}$ for 3 h. The slurries were subjected to a vacuum treatment for 1 h for defoaming before casting. A doctor blade was used to cast green BCZYSm films (4 mm x 20 mm) on glass substrate (10 mm x 40 mm x 1 mm). The green films were dried stepwisely at $200 \text{ }^\circ\text{C}$ for 20 min, $300 \text{ }^\circ\text{C}$ for 20 min, and $400 \text{ }^\circ\text{C}$ for 20 min using a hotplate.

The laser sintering apparatus of the authors group has been reported elsewhere. [10,12] A 100-W-class CO_2 laser ($\lambda = 10.6 \text{ }\mu\text{m}$, Ti100W, Synrad) was used for the sintering. No focal lens was used for this study. The samples were mounted to have 3-mm gap to a sample stage to avoid heat dissipation. Phases of the sintered samples were analyzed by X-ray diffraction (XRD, MiniFlex600, Rigaku). XRD patterns were collected by $\theta - 2\theta$ continuous scans using Cu-K α radiation ($\lambda = 1.5406 \text{ \AA}$). Microstructure of the samples were observed by field emission scanning electron microscope (FE-SEM) combined with energy dispersive spectrometer (EDS) (S-4800, Hitachi). Pt was coated on the samples by DC sputtering (Hummer 6.2, Anatech Ltd.) for 2 min under 80 mTorr to prevent charging up during SEM observation. Surface composition of the samples was analyzed by X-ray photoelectron spectroscopy (XPS, PHI 5000 VersaProbe III, ULVAC-PHI). XPS peak positions were corrected using a carbon as reference set at 284.80 eV. Temperature dependence of electric conductivity was measured using a potentio-galvanostat (SI1287, Solartron) and an impedance analyzer (SI1260, Solartron) under wet air humidified at $25 \text{ }^\circ\text{C}$ ($\approx 3.1 \text{ vol}\%\text{H}_2\text{O}$). Ag paste (T-20GM, Heraeus) and Ag wire ($\phi 0.1 \text{ mm}$, Alfa Aesar) were utilized as a current corrector and for connection between the samples and the potentio-galvanostat. The BCZYSm films were heated at $600 \text{ }^\circ\text{C}$ for 30 min and then were cooled in a step-wise manner down to $300 \text{ }^\circ\text{C}$ by $50 \text{ }^\circ\text{C}$ increments while measuring the conductivity at each temperature.

3. Results and discussion

Utilizing the aprotic and non-polar saturated hydrocarbon for the slurry solvent as an alternative to protic polar solvents is expected to lead to less formation of bulky polyanion chemicals from proton-conducting ceramics, resulting in less cracking with the laser sintering process. In order to clarify the role of saturated hydrocarbon, BCZYSm – *n*-hexadecane solution was prepared using a ball milling step, followed by chemical analysis of the barium content in the solvent. BCZYSm was chosen as one of the state-of-art proton-conducting ceramics, and *n*-hexadecane was chosen because it has the lowest vapor pressure and the highest flash point among all liquid hydrocarbons at room temperature. Solutions of BCZYSm – distilled water and isopropanol were also prepared for comparison. Fig. 2 shows the barium concentration in the three solvents. Hexadecane dissolves 1000 times less Ba^{2+} than water, demonstrating its inertness to the proton-conducting ceramics. It is noted that isopropanol also dissolved little barium. This implies that the formation of barium alkoxides is less likely to take place in the case of BCZYSm compared to solid state Li-conducting ceramic electrolytes such as the garnet system Al-doped $\text{Li}_7\text{La}_3\text{Zr}_2\text{O}_{12}$. [32] Nevertheless, the use of hydrophobic hexadecane will be better than that of the hydrophilic alcohols because the hydrophilic solvents absorb moisture rapidly once they are exposed to air. [33]

In order to develop the hexadecane-based BCZYSm slurry, the appropriate binder and surfactant materials have to be found.

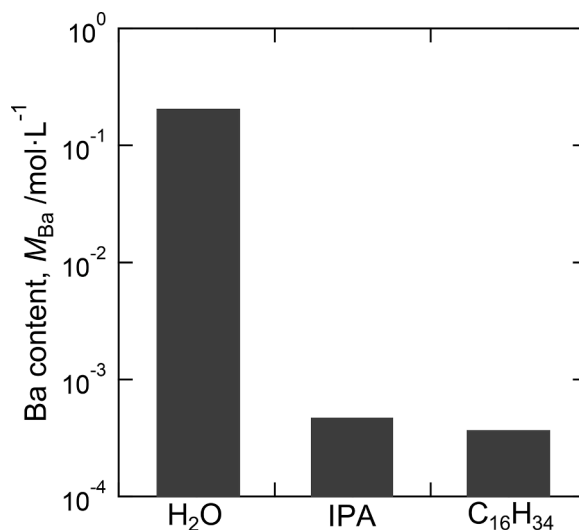


Fig. 2. Barium content in water (H_2O), isopropanol (IPA), and *n*-hexadecane ($\text{C}_{16}\text{H}_{34}$) after ball milling with BCZYSm.

Conventional binders and surfactants are rather hydrophilic therefore are insoluble in highly hydrophobic hexadecane. The authors found that polybutene and stearic acid, shown in Fig. 3(a), can be used as the binder and surfactant in the hexadecane-based slurry as follows.

For binders, the authors tried to use various hydrophobic polymers: poly(methyl methacrylate), polystyrene, and special PVB (polyvinyl butyral) having little OH content (B HH series, kuraray). However, none of these could be dissolved into hot hexadecane heated up even to that its evaporation becomes apparent ($\approx 150 \text{ }^\circ\text{C}$). This indicates that matching of hydrophobicity, but also polarity is an important criteria for dissolution. Therefore, polybutene which is a semi-solid polymer comprised of saturated hydrocarbon similar to hexadecane was the focus of subsequent studies. The authors confirmed that various ratios of polybutene – hexadecane solution can be prepared even using polybutene with large molecular weight ($\approx 6000 \text{ g}\cdot\text{mol}^{-1}$, Indopol® H-18,000, INEOS Oligomers). As shown in Fig. 3(b), at the volume ratio of polybutene: hexadecane around 3:4 to 1:1, the slurry shows appropriate characteristics for uniform casting, controlling green-film thickness, and prevention of cracking during the drying and sintering process.

In regard to surfactant material candidates, long-chain saturated fatty acids works well for saturated-hydrocarbon-based BCZYSm slurry due to structure induced increase in hydrophobicity and decreased polarity. Myristic ($\text{C}_{13}\text{H}_{27}\text{COOH}$), palmitic ($\text{C}_{15}\text{H}_{31}\text{COOH}$), and stearic ($\text{C}_{17}\text{H}_{35}\text{COOH}$) acids can be dissolved well in hexadecane. Since their hydroxyl branches are slightly polarized ($\text{H}^{\delta+}-\text{O}^{\delta-}$) and they are very weak acids ($\text{p}K_{\text{a}} \approx 6-7$ [42]), their hydroxyl branches can adhere to the ceramics surface but not induce chemical reactions. The authors confirmed that grain agglomeration of the BCZYSm powder in hexadecane was greatly reduced by the addition of stearic acid, as shown in Fig. 3(b). The amount of stearic acid should be kept small, e.g. 0.2 g respect to 15 mL of hexadecane, to inhibit foam production in the slurry.

The following experiment was conducted using this newly developed saturated-hydrocarbon-based slurry comprised of BCZYSm green powder 50 g, *n*-hexadecane 15 mL, large-molecular-weight polybutene 15 mL, and stearic acid 0.2 g. Even though more than 100 green films were cast using this slurry and were dried quickly, no samples exhibited cracking. The origin of the improved processing performance is believed to be negligible barium dissolution from BCZYSm to saturated-hydrocarbon-based organics and inhibition of the formation of polyanion chemicals.

Laser sintering was conducted for the green BCZYSm films casted in dimensions of 20 mm long, 4 mm width, $600 \text{ }\mu\text{m}$ thick (which is reduced to approximately $200 \text{ }\mu\text{m}$ after drying) on glass substrates. The scanning

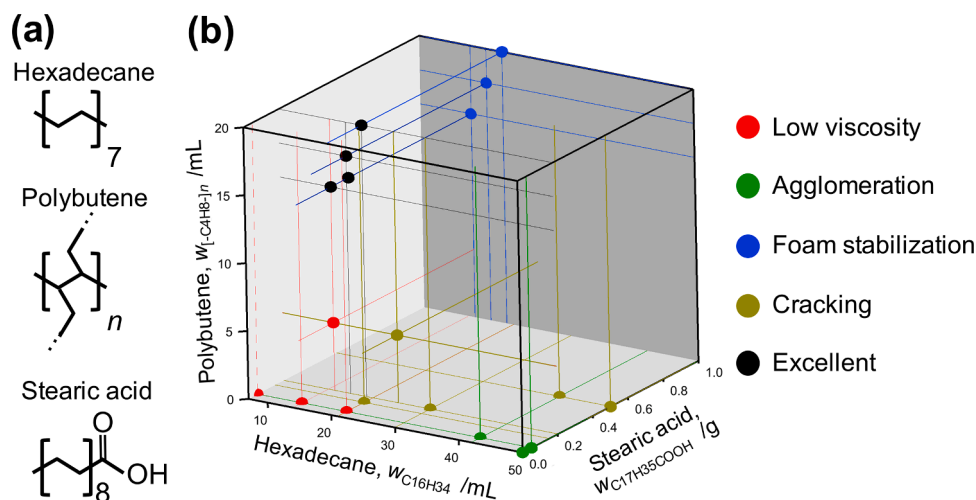


Fig. 3. (a) Organic materials used for saturated-hydrocarbon-based BCZYSm slurry, and (b) character of slurry containing green BCZYSm powder 50 g as functions of their concentrations.

was conducted on the longitudinal direction of the samples. As shown in Fig. 4(a), various sets of laser power and scanning speed was examined since their control is important for uniform sintering as the authors reported previously. [12] Laser-sintering conditions can be divided into several regions from the viewpoint of sintering behavior. In region 1, the laser power was weak and the scanning speed was fast, which resulted in insufficient heating for the sintering reaction. Even after laser sintering in this region, the BCZYSm membranes maintained their original whitish color, were observed to be very fragile and developed cracks upon removal from the substrate, as shown in Fig. 4(b). In region 2, the thermal energy given by the laser was high enough to sinter the air side while insufficient to densify the substrate side. This led to severe curving up of the sample as shown in Fig. 4(b). Uniform sintering of the samples through the air side to the substrate side was achieved in region 3. The BCZYSm membranes sintered at this condition region turned black, indicating that perovskite-type BCZYSm doped with Ni (sintering aid) was formed (their XRD patterns are shown later in Fig. 5(b)). [11] Laser sintering conducted near the boundary to region 2 resulted in membranes displaying no apparent cracks. Samples were durable enough for handling, as shown in Fig. 4(b). This narrow processing window is most

likely due to 1) an interdiffusion of BCZYSm with the underlying glass substrate and 2) laser ablation. A fusion of the BCZYSm membrane with the underlying glass was observed by a further increase in the laser power and/or a decrease scanning speed in region 4. This interdiffusion is likely taken place to a certain degree even in region 3 (its details are mentioned in next paragraph). The laser ablation phenomenon is clearly taken place at severely high power conditions (in the neighborhood of $\geq 75\%$) and it results only in thin and cracked BCZYSm membranes.

Further analysis was conducted to reveal the details about the interaction between the BCZYSm membranes and glass substrate during the laser sintering. Fig. 5(a) shows a cross-sectional SEM image of the BCZYSm membrane sintered under the laser conditions in region 3 (69% and $1 \text{ mm} \cdot \text{sec}^{-1}$). Clearly, the sample substrate side is more porous than its air side. XPS analysis revealed that the substrate and air sides contain 0.5 and 0.2 mol% silicon, respectively. This is consistent with a XRD patterns of them shown in Fig. 5(b). It indicates that more silicates were formed in the substrate side than in the air side. These results suggest that silicon is diffused from the glass to the BCZYSm substrate during laser sintering and prevented densification.

The interaction with substrate is a problem frequently observed for

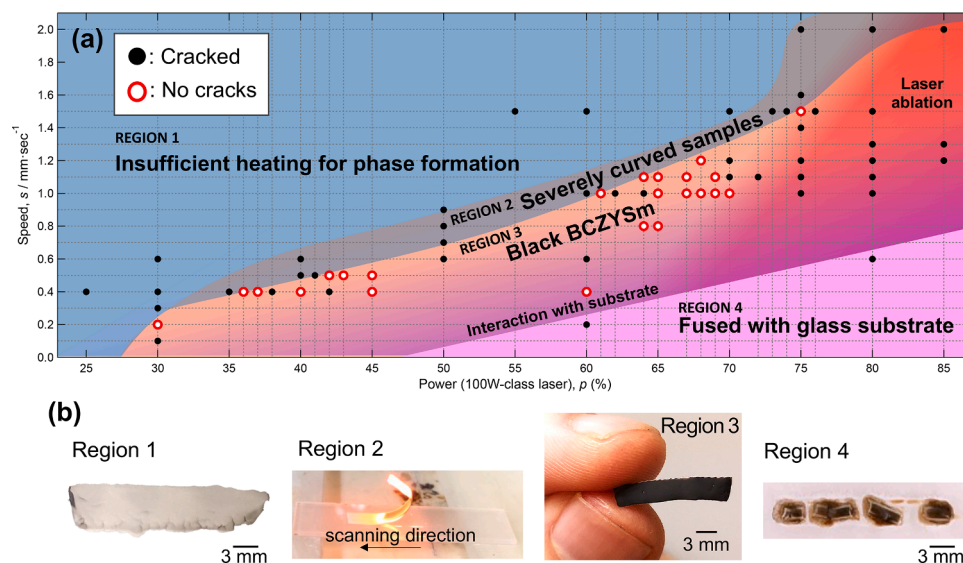


Fig. 4. (a) Laser power–speed diagram for sintering of BCZYSm membranes derived from saturated-hydrocarbon-based slurry, and (b) appearance of samples prepared in each region. The solid and open circles in (a) correspond to sample preparation conditions.

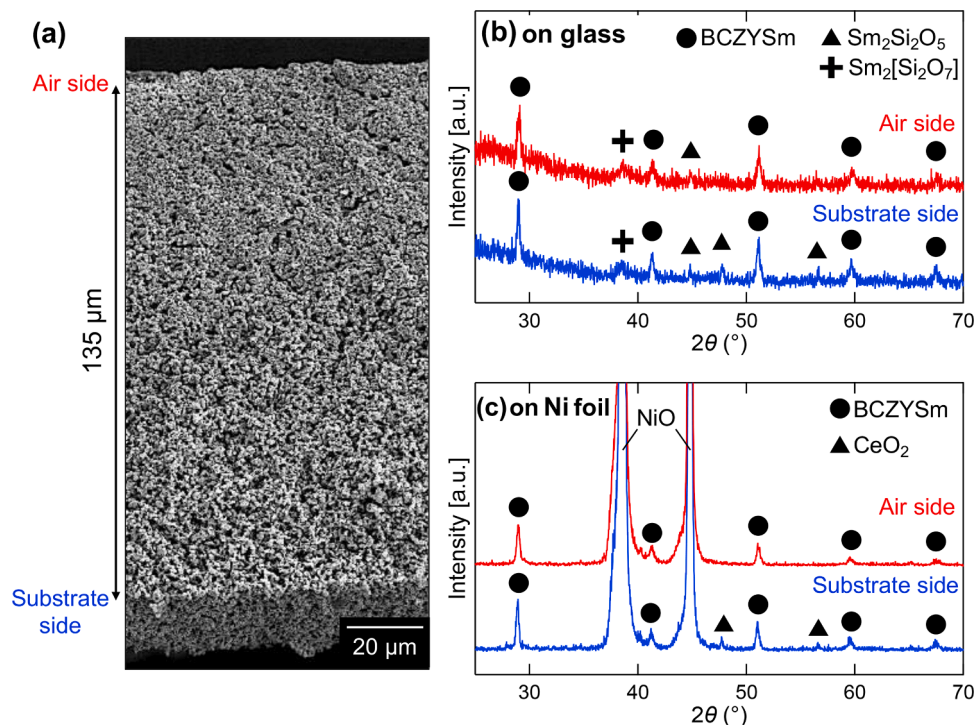


Fig. 5. (a) Cross-sectional SEM image and (b) XRD patterns of BCZYSm membrane sintered on glass, and (c) XRD patterns of BCZYSm membrane sintered on nickel foil. They were sintered at laser conditions in region 3 shown in Fig. 4(a).

laser sintering. The authors faced similar problems while laser sintering of Sr-doped LaCrO_3 interconnect membranes resulting in careful selection of appropriate substrate materials. [12] Likewise, the compatibility of the following substrate materials was examined for the laser sintering of BCZYSm membranes: aluminum foil, alumina plate, stainless steel plate, copper plate, and nickel foil. Although a perfectly compatible substrate material could not be found because of the complex quinary composition of BCZYSm, the nickel foil showed a relatively small degree of the interaction. Fig. 5(c) shows XRD patterns of the substrate and air sides of the BCZYSm membrane sintered on the nickel foil. Perovskite-type BCZYSm was observed with an oxidized substrate, NiO. The small amount of CeO_2 was also observed only for the substrate side,

which is presumably due to formation of NiO— CeO_2 solid solution [43] during laser heating followed by a phase separation as cooling down. Indeed, 3.9 and 4.7 wt%Ni were detected by XPS on the air and substrate sides of the BCZYSm membrane, which nickel contents are distinctly higher than the nominal content (1.0 wt%) added as sintering aid. Even though laser sintering on the nickel foil resulted in less formation of secondary phases as compared to glass, dense BCZYSm membranes could still not be prepared on the nickel foil owing to the nickel diffusion from it to the BCZYSm membrane which extracts cerium from the BCZYSm crystals.

Following a hypothesis that the interaction between the BCZYSm and nickel foil could be suppressed by a reduction in the contact area, a foam

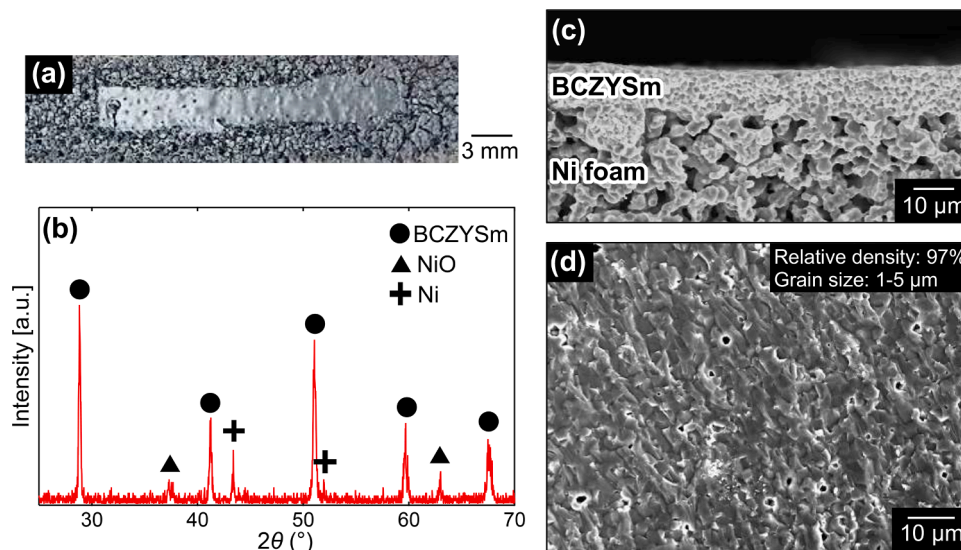


Fig. 6. (a) Appearance, (b) XRD pattern, (c) cross-sectional and (d) surface SEM images of BCZYSm membrane sintered on nickel foam. They were sintered at laser conditions in region 3 shown in Fig. 4(a).

of nickel (10 mm x 40 mm x 1.6 mm, $\geq 95\%$ porosity, MTT) was used as substrate. The foam was fine (hole diameters: 250 μm) enough to hold the slurry and green BCZYSm films could be cast in a similar manner as employed on nickel foil followed by laser sintering as shown in Fig. 6(a). An XRD pattern of the sample shows no secondary phases except for the partially oxidized substrate (Ni and NiO), as shown in Fig. 6(b). This is most likely because the interdiffusion between NiO and CeO₂ was prohibited due to the limited interface area between NiO and the BCZYSm film. The sintered BCZYSm film was 13.5 mm thick as shown in Fig. 6(c), which is an ideal thickness for electrolytes. This BCZYSm film was well densified as shown in Fig. 6(d) with a relative density of 97% by image analysis using GIMP. [44] This highly densified microstructure supports the hypothesis that the interaction between the BCZYSm film and substrate during laser sintering was suppressed by utilizing the foam-type substrate. However, smaller heat capacity of the Ni foam substrate and smaller heat transfer between substrate and membrane compared to the case of using the Ni foil may also be keys for the densification and single-phase formation.

For the laser-sintered BCZYSm film on nickel foam, electrochemical AC impedance measurement was carried out to clarify its quality as a proton-conducting electrolyte. The sample was reduced under 5%H₂ at 600 °C to minimize the influence from NiO of oxidized portion of substrate on the impedance spectra. The AC voltage was applied across the sample substrate side to air side. Fig. 7(a) shows the impedance spectra measured under humidified air. The spectrum at 600 °C is comprised of a slightly-visible arc which corresponds to bulk and grain-boundary resistance (shown as $R_{\text{bulk}} + R_{\text{G.B.}}$ in Fig. 7(a)) at high frequency side and a distorted arc which corresponds to polarization resistance at low frequency side. The electrode of this sample is different for each side (Ni and Ag), that leads the shape distortion of the low-frequency-side arc. As decreasing temperature, the bulk and grain-boundary resistance and the polarization resistance were both increased as is well known. The shape of the arc attributed to the polarization resistance was also changed, which implies some reactions were taken place at the interface and/or electrodes but its detail is unclear at this moment.

An Arrhenius-type plot for the ionic conductivity, σ , of the laser-sintered BCZYSm membrane is shown in Fig. 7(b). The $\log[\sigma]$ shows liner relationship with inverse temperature although it is slightly

scattered presumably due to the influence of the electrode resistance. The activation energy of the conductivity, calculated by the Arrhenius-type plot for $\ln[\sigma T/S \cdot \text{cm}^{-1} \cdot \text{K}]$, is 0.41 ± 0.05 eV. As shown in Fig. 7(c), this activation energy is similar to the BCZYSm pellet, suggesting protonic conduction of the laser-sintered BCZYSm membrane. The proton conductivity of the laser-sintered BCZYSm is on the order of 10^{-4} S $\cdot\text{cm}^{-1}$ at 600 °C that is approximately 10^2 times lower than that of BCZYSm pellet sintered using a conventional furnace. [3] It is general that film materials show lower conductivity than bulk materials due to difficulty of sintering. [12,45,46] In the case of this study, taking the 97% density into account, relatively low conductivity of the laser-sintered BCZYSm film is due not to insufficient densification but due most likely to its smaller grains (1–5 μm , Fig. 6(c)(d)) compared to the furnace-sintered BCZYSm pellet (20–50 μm). The authors have reported that the BCZYSm pellet shows approximately 50 times smaller conductivity when it is comprised of grains in 5–20 μm . [3] Preparation of the BCZYSm membranes comprised of well-grown grains may be possible by increasing thermal energy input from the laser. However, as shown in Fig. 4 and Fig. 5, this leads to chemical reactions with substrate. In addition, the laser heating may have technically been insufficient or oversufficient for the phase formation of BCZYSm, which can be an another reason of the relatively low conductivity of the laser-sintered BCZYSm. It has been reported in the Y-doped BaZrO₃ system that a sintering window (temperature and duration) is narrow in reality because of two-phase equilibrium state and barium sublimation even though they are hardly detected by XRD analysis, and its conductivity is decreased in 50 times by sintering under inappropriate temperature and duration combinations. [47,48] The authors group is trying to monitor the sample temperature during the laser sintering. Even with the difficulties encountered, it is worthwhile to continue development of the laser sintering process. The laser sintering of this BCZYSm membrane was completed in three seconds, which is more than million-fold shorter compared with the conventional sintering using furnace (typically takes ten-plus hours).

This study developed the chemically inert hydrocarbon-based slurry for mitigation of the cracking problem on the laser sintering of the thin proton-conducting electrolytes. By utilizing this slurry, rapid laser sintering of 13.5-mm-thick BCZYSm membrane was achieved. The authors

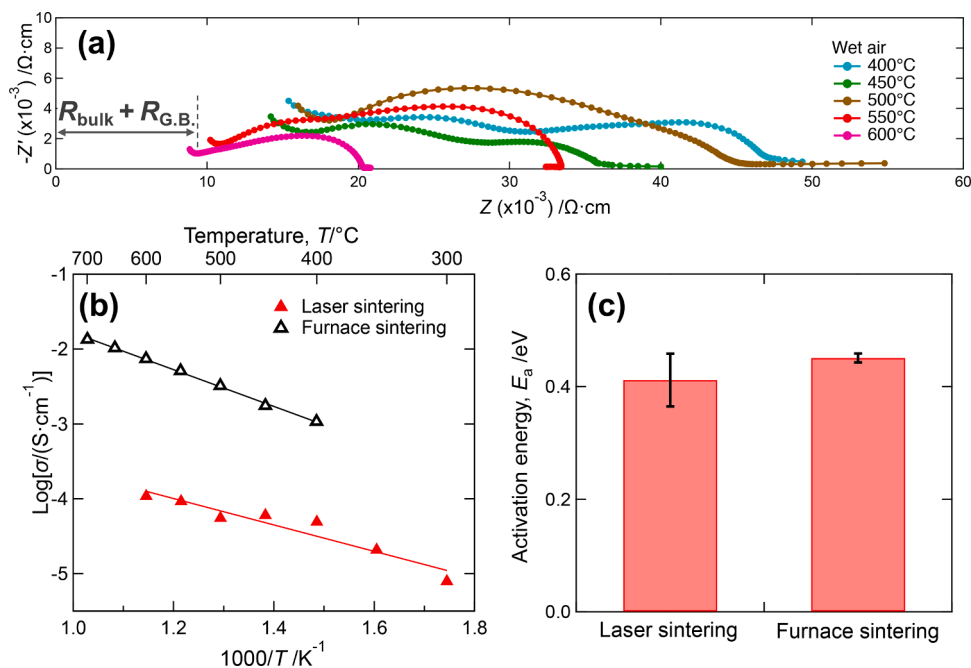


Fig. 7. (a) Nyquist plot, (b) ionic conductivity and (c) activation energy of laser-sintered BCZYSm membrane measured under humidified air. Conductivity and activation energy for furnace-sintered BCZYSm [3] are also shown for comparison.

believe that this slurry can be also used for wet processing of the basic ceramics membranes in the other fields such as lithium-ion batteries, sodium-ion batteries, and KNbO₃-based ferroelectric materials [49]. Although this study used the purified *n*-hexadecane for solvent, mixture of the saturated higher hydrocarbons (so-called liquid paraffin or white mineral oil) can likely used as an economical and practical alternation because it has almost same properties. The saturated-hydrocarbon-based slurries will facilitate the wet processing and rapid laser sintering of not only the proton-conducting ceramic electrolytes but also various functional ceramic membranes.

4. Conclusions

Commercialization of the ceramic fuel cells and electrolyzers has been hindered by production difficulty arise from refractory nature of proton-conducting BaZrO₃-BaCeO₃-based electrolytes. The process of rapid laser sintering of the thin electrolytes has been therefore attractive; however, cracking caused by chemical reactions between basic ceramic constituents and the polar solvents during wet processing has been a problematic. This study mitigated this issue by developing the chemically inert slurry comprised of highly hydrophobic hexadecane, polybutene, and stearic acid. The 97% dense BaCe_{0.7}Zr_{0.1}Y_{0.07}Sm_{0.13}O_{3-δ} membrane in 20 mm long, 4 mm wide, and 13.5 μm thick and showing proton conductivity on the order of 10⁻⁴ S•cm⁻¹ at 600 °C, was successfully prepared on nickel foam in just three seconds by the laser sintering with the optimized slurry compositions and laser operation conditions. This study points out that the impact of the chemical reaction between ceramic constituents and solvents on the wet processing has to be taken into consideration, and the use of the hydrophobic slurry will beneficial especially for handling the proton-conducting ceramic membranes.

Disclaimer

"This report was prepared as an account of work sponsored by an agency of the United States Government. Neither the United States Government nor any agency thereof, nor any of their employees, makes any warranty, express or implied, or assumes any legal liability or responsibility for the accuracy, completeness, or usefulness of any information, apparatus, product, or process disclosed, or represents that its use would not infringe privately owned rights. Reference herein to any specific commercial product, process, or service by trade name, trademark, manufacturer, or otherwise does not necessarily constitute or imply its endorsement, recommendation, or favoring by the United States Government or any agency thereof. The views and opinions of authors expressed herein do not necessarily state or reflect those of the United States Government or any agency thereof."

Declaration of Competing Interest

The authors declare the following financial interests/personal relationships which may be considered as potential competing interests:

Jianhua Tong, Kyle Brinkman reports financial support was provided by US Department of Energy. Fei Peng, Hai Xiao reports financial support was provided by US Department of Energy.

Acknowledgement

This material is based upon work supported by the U.S. Department of Energy's Office of Energy Efficiency and Renewable Energy (EERE) under the Hydrogen and Fuel Cell Technologies Office Award Number DE-EE0008428. The authors would like to acknowledge Dr. Estes for her support for the ICP-MS analysis. The authors are grateful to the Electron Microscopy Facility at Clemson University. The authors are also grateful to INEOS oligomers and Kuraray for supplying polybutenes and PVBs, respectively.

References

- [1] C. Zuo, S. Zha, M. Liu, M. Hatano, M. Uchiyama, Ba(Zr_{0.1}Ce_{0.7}Y_{0.2}O_{3-δ}) as an Electrolyte for Low-Temperature Solid-Oxide Fuel Cells, *Adv. Mater.* 18 (2006) 3318–3320, <https://doi.org/10.1002/adma.200601366>.
- [2] L. Yang, S. Wang, K. Blinn, M. Liu, Z. Liu, Z. Cheng, M. Liu, Enhanced Sulfur and Coking Tolerance of a Mixed Ion Conductor for SOFCs: BaZr_{0.1}Ce_{0.7}Y_{0.2-*x*}Yb_{*x*}O_{3-δ}, *Science* 326 (2009) 126–129, <https://doi.org/10.1126/science.1174811>.
- [3] Y. Meng, J. Gao, H. Huang, M. Zou, J. Duffy, J. Tong, K.S. Brinkman, A high-performance reversible protonic ceramic electrochemical cell based on a novel Sm-doped BaCe_{0.7}Zr_{0.1}Y_{0.2}O_{3-δ} electrolyte, *J. Power Sources* 439 (2019), 227093, <https://doi.org/10.1016/j.jpowsour.2019.227093>.
- [4] J. Hyodo, K. Kitabayashi, K. Hoshino, Y. Okuyama, Y. Yamazaki, Fast and Stable Proton Conduction in Heavily Scandium-Doped Polycrystalline Barium Zirconate at Intermediate Temperatures, *Adv. Energy Mater.* 10 (2020), 2000213, <https://doi.org/10.1002/aenm.202000213>.
- [5] J. Tong, D. Clark, L. Bernau, M. Sanders, R. O'Hayre, Solid-state reactive sintering mechanism for large-grained yttrium-doped barium zirconate proton conducting ceramics, *J. Mater. Chem.* 20 (2010) 6333–6341, <https://doi.org/10.1039/C0JM00381F>.
- [6] S. Nikodemski, J. Tong, R. O'Hayre, Solid-state reactive sintering mechanism for proton conducting ceramics, *Solid State Ionics* 253 (2013) 201–210, <https://doi.org/10.1016/j.ssi.2013.09.025>.
- [7] S. Mu, Z. Zhao, J. Lei, Y. Hong, T. Hong, D. Jiang, Y. Song, W. Jackson, K. S. Brinkman, F. Peng, H. Xiao, J. Tong, Engineering of microstructures of protonic ceramics by a novel rapid laser reactive sintering for ceramic energy conversion devices, *Solid State Ionics* 320 (2018) 369–377, <https://doi.org/10.1016/j.ssi.2018.03.023>.
- [8] Y. Hong, J. Lei, M. Heim, Y. Song, L. Yuan, S. Mu, R.K. Bordia, H. Xiao, J. Tong, F. Peng, Fabricating ceramics with embedded microchannels using an integrated additive manufacturing and laser machining method, *J. Am. Ceram. Soc.* 102 (2019) 1071–1082, <https://doi.org/10.1111/jace.15982>.
- [9] S. Mu, Y. Hong, H. Huang, A. Ishii, J. Lei, Y. Song, Y. Li, K.S. Brinkman, F. Peng, H. Xiao, J. Tong, A Novel Laser 3D Printing Method for the Advanced Manufacturing of Protonic Ceramics, *Membranes* 10 (2020) 98, <https://doi.org/10.3390/membranes10050098>.
- [10] S. Mu, H. Huang, A. Ishii, Y. Hong, A. Santomauro, Z. Zhao, M. Zou, F. Peng, K. S. Brinkman, H. Xiao, J. Tong, Rapid Laser Reactive Sintering for Sustainable and Clean Preparation of Protonic Ceramics, *ACS Omega* 5 (2020) 11637–11642, <https://doi.org/10.1021/acsomega.0c00879>.
- [11] S. Mu, H. Huang, A. Ishii, Z. Zhao, M. Zou, P. Kuzbary, F. Peng, K.S. Brinkman, H. Xiao, J. Tong, Rapid laser reactive sintering of BaCe_{0.7}Zr_{0.1}Y_{0.1}Yb_{0.1}O_{3-δ} electrolyte for protonic ceramic fuel cells, *J. Power Sources Adv.* 4 (2020), 100017, <https://doi.org/10.1016/j.jpowers.2020.100017>.
- [12] A. Ishii, S. Mu, Y. Meng, H. Huang, J. Lei, Y. Li, F. Peng, H. Xiao, J. Tong, K. S. Brinkman, Rapid Laser Processing of Thin Sr-Doped LaCrO_{3-δ} Interconnects for Solid Oxide Fuel Cells, *Energy Technol* 8 (2020), 2000364, <https://doi.org/10.1002/ente.202000364>.
- [13] S. Mu, Z. Zhao, H. Huang, J. Lei, F. Peng, H. Xiao, K.S. Brinkman, J. (Joshua) Tong, Advanced Manufacturing of Intermediate-Temperature Protonic Ceramic Electrochemical Cells, *Electrochem. Soc. Interface* 29 (2020) 67, <https://doi.org/10.1149/2.F09204IF>.
- [14] S. Fang, S. Wang, K.S. Brinkman, Q. Su, H. Wang, F. Chen, Relationship between fabrication method and chemical stability of Ni–BaZr_{0.8}Y_{0.2}O_{3-δ} membrane, *J. Power Sources* 278 (2015) 614–622, <https://doi.org/10.1016/j.jpowsour.2014.12.108>.
- [15] T. Ishiyama, H. Kishimoto, K. Develos-Bagarinao, K. Yamaji, T. Yamaguchi, Y. Fujishiro, Decomposition reaction of BaZr_{0.1}Ce_{0.7}Y_{0.1}Yb_{0.1}O_{3-δ} in carbon dioxide atmosphere with nickel sintering aid, *J. Ceram. Soc. Jpn.* 125 (2017) 247–251, <https://doi.org/10.2109/jcersj2.16281>.
- [16] Y. Yang, Y. Zeng, B.S. Amirkhiz, J.-L. Luo, N. Yan, Promoting the ambient-condition stability of Zr-doped barium cerate: toward robust solid oxide fuel cells and hydrogen separation in syngas, *J. Power Sources* 378 (2018) 134–138, <https://doi.org/10.1016/j.jpowsour.2017.12.036>.
- [17] A. Sharafi, S. Yu, M. Naguib, M. Lee, C. Ma, H.M. Meyer, J. Nanda, M. Chi, D. J. Siegel, J. Sakamoto, Impact of air exposure and surface chemistry on Li–Li₃La₃Zr₂O₁₂ interfacial resistance, *J. Mater. Chem. A.* 5 (2017) 13475–13487, <https://doi.org/10.1039/C7TA03162A>.
- [18] T. Allison, JANAF Thermochemical Tables, NIST Standard Reference Database 13 (1996), <https://doi.org/10.18434/T42531>.
- [19] SpringerMaterials, Thermodynamic Properties of Compounds, CaB₆ to BaO–WO₃, in: Landolt-Börnstein - Group IV Physical Chemistry 19A1, Springer-Verlag, Berlin/Heidelberg, 1999, pp. 375–400, https://doi.org/10.1007/10652891_19 (accessed February 15, 2021).
- [20] C.W. Tanner, A.V. Virkar, Instability of BaCeO₃ in H₂O-Containing Atmospheres, *J. Electrochem. Soc.* 143 (1996) 1386, <https://doi.org/10.1149/1.1836647>.
- [21] M.D. Gonçalves, P.S. Maram, R. Muccillo, A. Navrotsky, Enthalpy of formation and thermodynamic insights into yttrium doped BaZrO₃, *J. Mater. Chem. A.* 2 (2014) 17840–17847, <https://doi.org/10.1039/C4TA03487B>.
- [22] A. Sanson, P. Pinasco, E. Roncari, Influence of pore formers on slurry composition and microstructure of tape cast supporting anodes for SOFCs, *J. Eur. Ceram. Soc.* 28 (2008) 1221–1226, <https://doi.org/10.1016/j.jeurceramsoc.2007.10.001>.
- [23] N. Ai, Z. Lü, K. Chen, X. Huang, Y. Liu, R. Wang, W. Su, Preparation of Sm_{0.2}Ce_{0.8}O_{1.9} membranes on porous substrates by a slurry spin coating method and its application in IT-SOFC, *J. Membr. Sci.* 286 (2006) 255–259, <https://doi.org/10.1016/j.memsci.2006.10.003>.

- [24] Y. Hayamizu, M. Kato, H. Takamura, Effects of surface modification on the oxygen permeation of $\text{Ba}_{0.5}\text{Sr}_{0.5}\text{Co}_{0.8}\text{Fe}_{0.2}\text{O}_{3-\delta}$ membrane, *J. Membr. Sci.* 462 (2014) 147–152, <https://doi.org/10.1016/j.memsci.2014.03.038>.
- [25] T. Yamaguchi, H. Shimada, U. Honda, H. Kishimoto, T. Ishiyama, K. Hamamoto, H. Sumi, T. Suzuki, Y. Fujishiro, Development of anode-supported electrochemical cell based on proton-conductive $\text{Ba}(\text{Ce},\text{Zr})\text{O}_3$ electrolyte, *Solid State Ionics* 288 (2016) 347–350, <https://doi.org/10.1016/j.ssi.2015.12.007>.
- [26] C. Hänsel, S. Afyon, J.L.M. Rupp, Investigating the all-solid-state batteries based on lithium garnets and a high potential cathode— $\text{LiMn}_{1.5}\text{Ni}_{0.5}\text{O}_4$, *Nanoscale* 8 (2016) 18412–18420, <https://doi.org/10.1039/C6NR06955J>.
- [27] S. Lee, I. Park, H. Lee, D. Shin, Continuously gradient anode functional layer for BCZY based proton-conducting fuel cells, *Int. J. Hydrog. Energy* 39 (2014) 14342–14348, <https://doi.org/10.1016/j.ijhydene.2014.03.135>.
- [28] X. Yan, Z. Li, Z. Wen, W. Han, $\text{Li}/\text{Li}_7\text{La}_3\text{Zr}_2\text{O}_{12}/\text{LiFePO}_4$ All-Solid-State Battery with Ultrathin Nanoscale Solid Electrolyte, *J. Phys. Chem. C* 121 (2017) 1431–1435, <https://doi.org/10.1021/acs.jpcc.6b10268>.
- [29] X. Yan, Z. Li, H. Ying, F. Nie, L. Xue, Z. Wen, W.-Q. Han, A novel thin solid electrolyte film and its application in all-solid-state battery at room temperature, *Ionics (Kiel)* 24 (2018) 1545–1551, <https://doi.org/10.1007/s11581-017-2353-x>.
- [30] J.-H. Choi, C.-H. Lee, J.-H. Yu, C.-H. Doh, S.-M. Lee, Enhancement of ionic conductivity of composite membranes for all-solid-state lithium rechargeable batteries incorporating tetragonal $\text{Li}_7\text{La}_3\text{Zr}_2\text{O}_{12}$ into a polyethylene oxide matrix, *J. Power Sources* 274 (2015) 458–463, <https://doi.org/10.1016/j.jpowsour.2014.10.078>.
- [31] D.H. Kim, M.Y. Kim, S.H. Yang, H.M. Ryu, H.Y. Jung, H.-J. Ban, S.-J. Park, J. S. Lim, H.-S. Kim, Fabrication and electrochemical characteristics of NCM-based all-solid lithium batteries using nano-grade garnet Al-LLZO powder, *J. Ind. Eng. Chem.* 71 (2019) 445–451, <https://doi.org/10.1016/j.jiec.2018.12.001>.
- [32] R. Kun, F. Langer, M. Delle Piane, S. Ohno, W.G. Zeier, M. Gockeln, L. Colombi Ciacchi, M. Busse, I. Fekete, Structural and Computational Assessment of the Influence of Wet-Chemical Post-Processing of the Al-Substituted Cubic $\text{Li}_7\text{La}_3\text{Zr}_2\text{O}_{12}$, *ACS Appl. Mater. Interfaces* 10 (2018) 37188–37197, <https://doi.org/10.1021/acsami.8b09789>.
- [33] B. Tan, P. Melius, P. Ziegler, A Simple Gas Chromatographic Method for the Study of Organic Solvents: moisture Analysis, Hygroscopicity, and Evaporation, *J. Chromatogr. Sci.* 20 (1982) 213–217, <https://doi.org/10.1093/chromsci/20.5.213>.
- [34] H. Shen, E. Yi, M. Amores, L. Cheng, N. Tamura, D.Y. Parkinson, G. Chen, K. Chen, M. Doeff, Oriented porous LLZO 3D structures obtained by freeze casting for battery applications, *J. Mater. Chem. A* 7 (2019) 20861–20870, <https://doi.org/10.1039/C9TA06520B>.
- [35] H. Lee, S. Lee, T. Lee, S. Park, D. Shin, Long term stability of porosity gradient composite cathode controlled by electro-static slurry spray deposition, *Int. J. Hydrog. Energy* 42 (2017) 3748–3752, <https://doi.org/10.1016/j.ijhydene.2016.09.077>.
- [36] W. Sun, N. Zhang, Y. Mao, K. Sun, Preparation of dual-pore anode supported Sc_2O_3 -stabilized- ZrO_2 electrolyte planar solid oxide fuel cell by phase-inversion and dip-coating, *J. Power Sources* 218 (2012) 352–356, <https://doi.org/10.1016/j.jpowsour.2012.06.107>.
- [37] H. Duan, Y.-X. Yin, Y. Shi, P.-F. Wang, X.-D. Zhang, C.-P. Yang, J.-L. Shi, R. Wen, Y.-G. Guo, L.-J. Wan, Dendrite-Free Li-Metal Battery Enabled by a Thin Asymmetric Solid Electrolyte with Engineered Layers, *J. Am. Chem. Soc.* 140 (2018) 82–85, <https://doi.org/10.1021/jacs.7b10864>.
- [38] I. Ismail, A.M.M. Jani, N. Osman, Microstructure control of SOFC cathode material: the role of dispersing agent, *AIP Conf. Proc.* 1877 (2017), 030004, <https://doi.org/10.1063/1.4999860>.
- [39] T. Baquero, J. Escobar, J. Frade, D. Hotza, Aqueous tape casting of micro and nano YSZ for SOFC electrolytes, *Ceram. Int.* 39 (2013) 8279–8285, <https://doi.org/10.1016/j.ceramint.2013.03.097>.
- [40] N. Osman, N.A. Mazlan, N.S.M. Affandi, N.W. Mazlan, A.M. Md Jani, Optimization of electrolyte performance by tailoring the structure and morphology of $\text{Ba}(\text{Ce},\text{Zr})\text{O}_3$ ceramics with different types of surfactants, *Ceram. Int.* 46 (2020) 27401–27409, <https://doi.org/10.1016/j.ceramint.2020.07.226>.
- [41] A. Akbari-Fakhrabadi, R.V. Mangalaraja, F.A. Sanhueza, R.E. Avila, S. Ananthakumar, S.H. Chan, Nanostructured Gd– CeO_2 electrolyte for solid oxide fuel cell by aqueous tape casting, *J. Power Sources* 218 (2012) 307–312, <https://doi.org/10.1016/j.jpowsour.2012.07.005>.
- [42] S. Skulj, M. Vazdar, Calculation of apparent pKa values of saturated fatty acids with different lengths in DOPC phospholipid bilayers, *Phys. Chem. Phys.* 21 (2019) 10052–10060, <https://doi.org/10.1039/C9CP01204D>.
- [43] H. Kaneko, Y. Tamaura, Reactivity and XAFS study on $(1-x)\text{CeO}_2-x\text{NiO}$ ($x=0.025-0.3$) system in the two-step water-splitting reaction for solar H₂ production, *J. Phys. Chem. Solids* 70 (2009) 1008–1014, <https://doi.org/10.1016/j.jpcs.2009.05.015>.
- [44] S. Kimball, P. Mattis, The GIMP team, GNU Image Manipulation Program 2.10.10, 2019 <https://www.gimp.org/> (accessed February 15, 2021).
- [45] G. Taillades, P. Pers, V. Mao, M. Taillades, High performance anode-supported proton ceramic fuel cell elaborated by wet powder spraying, *Int. J. Hydrog. Energy* 41 (2016) 12330–12336, <https://doi.org/10.1016/j.ijhydene.2016.05.094>.
- [46] K. Xie, R. Yan, Y. Jiang, X. Liu, G. Meng, A simple and easy one-step fabrication of thin $\text{BaZr}_{0.1}\text{Ce}_{0.7}\text{Y}_{0.2}\text{O}_{3-\delta}$ electrolyte membrane for solid oxide fuel cells, *J. Membr. Sci.* 325 (2008) 6–10, <https://doi.org/10.1016/j.memsci.2008.07.055>.
- [47] C. Hiraiwa, D. Han, A. Kuramitsu, A. Kuwabara, H. Takeuchi, M. Majima, T. Uda, Chemical Expansion and Change in Lattice Constant of Y-Doped BaZrO_3 by Hydration/Dehydration Reaction and Final Heat-Treating Temperature, *J. Am. Ceram. Soc.* 96 (2013) 879–884, <https://doi.org/10.1111/jace.12172>.
- [48] D. Han, T. Uda, Correlation between Phase Behavior and Electrical Conductivity of 10 mol% Y-Doped BaZrO_3 : an Anomalous Dispersion Effect-Aided Synchrotron Radiation XRD Study Combined with TEM Observation and Electrochemical Analysis, *ACS Appl. Mater. Interfaces* 11 (2019) 3990–4000, <https://doi.org/10.1021/acsami.8b19576>.
- [49] Y. Saito, H. Takao, T. Tani, T. Nonoyama, K. Takatori, T. Homma, T. Nagaya, M. Nakamura, Lead-free piezoceramics, *Nature* 432 (2004) 84–87, <https://doi.org/10.1038/nature03028>.